Experimental Wavelet Transient-State Analysis of Electrical Machines Directly Feeding by Photovoltaic Cells

NEVZAT ONAT
Vocational School of Technical Studies Electrical Programme
Marmara University
Göztepe Campus, 34722 Kadıköy – İstanbul
TURKEY
nonat@marmara.edu.tr

İSMAIL KIYAK GÖKHAN GÖKMEN
Department of Electrical Education
Marmara University
Technical Education Faculty, Göztepe Campus, 34722 Kadıköy – İstanbul
TURKEY
imkiyak@marmara.edu.tr gokhang@marmara.edu.tr

Abstract: - Solar electric systems -also known as photovoltaic (PV) systems- have very little impact on the environment, making them one of the cleanest power-generating technologies available. While they're operating, PV systems produce no air pollution, hazardous waste, or noise, and they require no transportable fuels. In PV System design, the selection and proper installation of appropriately-sized components directly affect system reliability, lifetime, and initial cost.
The features of the receivers fed from PV systems have a direct impact on the cells; namely, the power generators of the system. System behavior may change in receivers equipped with electrical machines fed from photovoltaic's, depending on the characteristics of the machine used. The fact that in the design phase of the photovoltaic systems which will feed electrical machines that the current drawn by any electrical machines at the startup is higher than the nominal operating current should be taken into account. In this study, the startup and nominal operating behaviors of electrical machines directly connected to photovoltaic system (not having any storage system or controller system) were empirically examined, obtained power values (in p.u.) were decomposed to sub-frequency components by means of the discrete wavelet transform than they were compared to each others.

Key-Words: - Photovoltaic Cells, Transient State, Electrical Machines, Wavelet Filter Bank, Multiresolution Analysis.

1 Introduction

As the conventional fossil fuel is depleting at a faster rate while the cost of electrical energy is increasing due to growing consumer demand, Photovoltaic (PV) energy becomes a promising renewable alternate source. The emerging renewable energy, Solar and wind are expected to play a major role in supplying at least 5-10% of total electrical energy demand worldwide. Over 2 billion people in the developing world have no access to electricity. For these people, PV is probably the most economical and abundant power source today. It is anticipated that within the next 10 years, PV solar arrays will become cost competitive with traditional power sources in countries with extensive electrical infrastructure (like the U.S. and Europe). They have the advantages of requiring less maintenance and air pollution free, but their installation cost is relatively high and in most cases they need a power conditioner (DC/DC or DC/AC) for motorized load-interface due to load non-linearity (V-I) relationship [1].
Still the PV modules have relatively low conversion efficiency; so more price can be reduced using high efficiency power conditioner that are designed to extract the maximum power from the PV module. The performance of a PV array system depends on the operating conditions as well as the solar cell and array design quality. The output voltage, current and power of a PV array vary as function of solar irradiation level, temperature and load current. So the combined effect of all these parameters should be considered while designing the PV array, so any change in the ambient temperature or irradiation affect the PV array output power. The least expensive method of converting solar energy into mechanical energy is direct interfacing of dc motors

with photovoltaic generators without using storage batteries. One of the most suitable systems to utilize solar energy is to use PV–DC motor to drive a water pump for storing water for subsequent use in various forms [1, 2]

The solar cell is a semiconductor device that converts the solar insolation directly to electrical energy. The cell is a non-linear device and can be represented by the $I-V$ terminal characteristics, or by an approximate electrical equivalent circuit as shown in Fig.1.

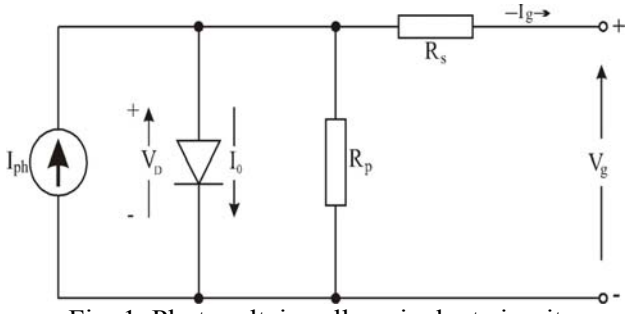

Fig. 1. Photovoltaic cell equivalent circuit

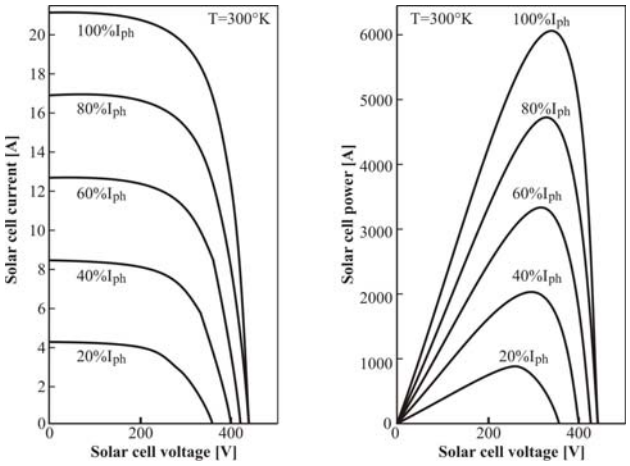

Fig. 2. Characteristics of a photovoltaic cell

The cells are connected in series and in parallel combinations in order to form an array of the desired voltage and power levels. Fig. 2 represents $I-V$ and $P-V$ characteristics of the solar-cell generator for five insolation levels (in percentages). The $I_g - V_g$ equation of the solar cell generator, which consists of N_s cells in series and N_p cells in parallel, is given by:

$$V_g = I_g R_s \frac{N_s}{N_p} \ln\left(1 + \frac{N_p I_{ph} - I_g}{N_p I_0}\right) \qquad (1)$$

$$I_g = I_{ph} - I_0\left(e^{\frac{qV_g}{kT}} - 1\right) \qquad (2)$$

Where, I_{ph} cell photocurrent (amps), proportional to the insolation; I_0 cell reverse saturation current; R_s cell series resistance; $q = 1.6x10^{-19} C$ electron charge, $k = 1.38x10^{-23} j/K$ Boltzmann's constant; and T absolute temperature [3, 4].

Fig. 2 shows that the PV cell has both a limiting voltage and a limiting current. Hence, the cell is not damaged by operating it under either open circuit or short circuit conditions. To determine the short circuit current of a PV cell, simply set $V_g = 0$ in the exponent. This leads $I_{SC} = I_{ph}$. To a very good approximation, the cell current is directly proportional to the cell irradiance. Thus; if the cell current is known under standard test conditions, $G = 1 kW/m^2$ at A.M.1.5, then the cell current at any other irradiance, G, is given by

$$I_{ph}(G) = \frac{G}{G_0} I_{ph}(G_0) \qquad (3)$$

To determine the open circuit voltage of the cell, the cell current is set to zero and Eq. 2 is solved V_{OC}, yielding the result

$$V_{OC} = \frac{kT}{q} \ln \frac{I_{ph} + I_0}{I_0} \cong \frac{kT}{q} \ln \frac{I_{ph}}{I_0} \qquad (4)$$

Since normally $I_{ph} >> I_0$. For example if the ratio of photocurrent to reverse saturation current is 10^{10}, using a thermal voltage (kT/q) of $26mV$, yields $V_{OC} = 0.6V$. Note that the open circuit voltage is only logarithmically dependent on the cell illumination, while the short circuit current is directly proportional to cell illumination.

The maximum power point may also be determined by differentiating the cell power equation and setting the result equal to zero. After finding the cell power equation is satisfied, and checking to verify that this voltage represents a maximum, maximum power point is known. The maximum power point is also readily found by simply plotting cell power versus cell voltage, as shown in Fig. 2 If I_m and V_m represents the cell current and voltage at maximum power respectively, then the cell maximum power can be expressed as,

$$P_{max} = I_m \cdot V_m = FF \cdot I_{SC} \cdot V_{OC} \qquad (5)$$

Where FF is defined as cell *fill factor*. The fill factor is a measure of the quality of the cell. Cell with large internal resistance will have smaller fill factors, while ideal cell will have a fill factor of unity. Note that a unity fill factor suggests a rectangular $I-V$ characteristic. Although a real cell does not have a rectangular characteristic, it is clear that it has a region where its operation approximates that of an ideal voltage source and another region where its operation approximates that of an ideal current source [5, 6]

Most PV systems are used for direct current (DC) electrical appliances because the current produced by a PV cell is basically of the DC type. However, DC electrical appliances are rarely found in everyday usage, and, moreover, it is not worthwhile converting existing alternating current (AC) electrical appliances for a PV power supply. Instead, an inverter is added to the PV system in order to convert the DC generated by the PV modules into AC type suitable for AC appliances [7].

2 Feeding of Electrical Machines from Photovoltaics

Photovoltaic systems have a high potential of application in various areas of today's world. The features of the receivers fed from PV systems have a direct impact on the cells; namely, the power generators of the system. Such impacts can be more evident particularly in the systems in which the load is directly connected to cells. It is well known that energy producing companies are obliged to supply excellent energy quality to the customers following the national and international limits and standards. High harmonic existence represents a possible source of faults and troubles for loads (motors, home electrical appliances, computer systems etc.) and for the electric system equipment (capacitors, cables etc.). All harmonic sources and effects have been well identified and presented in the past. The increased use of renewable energy sources and energy saving measures follow worldwide accepted strategic guidelines. Most renewable energy sources that produce electric power use power electronics (converters, inverters), which represent also a harmonic source [8, 9]. System behavior may change in receivers equipped with electrical machines fed from photovoltaics (water pumps and storage systems, cooling systems, ventilation systems, satellite systems, etc), depending on the characteristics of the machine used. It is possible to encounter some studies in the literature, which have been carried out on photovoltaic systems feeding electrical machines. Arrouf M. has worked on various control systems related with feeding of one and three-phase asynchronous (induction) motors from photovoltaics [10, 11]. Singer has examined startup characteristics of various DC machines fed from photovoltaics so as to make some suggestions aimed at improving performance [12]. To improve the performance of photovoltaic systems under AC loads, Sukamongkol Y. has worked on a computer simulation method [7]. Since the DC motors are used particularly in transportation system, they should be taken into account in designing transportation vehicles fed from photovoltaics. To achieve maximum performance from the DC motors to be used in such vehicles, various parameters should be taken into account [13].

The startup and nominal operating behaviors of electrical machines directly connected to photovoltaic system (not having any storage system or controller system) were empirically examined in this study.

Electrical machines are divided into two main categories: direct current and alternating current machines. DC motors fed from photovoltaic systems can be directly connected to the source. In some cases, it might be necessary to provide an inverter and rectifier to the system due to differences in voltage values. However, it is obligatory to use an inverter to feed alternating current machines. Therefore, the behavior of inverter circuit is effective on the systems of alternating current machines and should be considered.

The fact that in the design phase of the photovoltaic systems which will feed electrical machines that the current drawn by any electrical machines at the startup is higher than the nominal operating current should be taken into account. Due to the high current drawn at the startup, power consumption of the machine will be high as well. The amount of this "high current" changes from one machine to another. Even the machines of the same type can draw different startup currents due to different connection methods. For instance; Y-connected squirrel-cage induction machines draw currents 1.7-2 times higher than nominal currents while this value can be 4-5 times in delta connected squirrel-cage induction machines and around 1.3-1.6 times in wound rotor induction machines. Startup current of DC machines is considerably high. This current is limited by various starting systems. However, such starting systems are designed in such way to limit the starting current with 1.5-2 times of the nominal value [13, 14.

3 Problem Solution

One of the transient analysis methods is the wavelet transform. The wavelet transform is a recently developed mathematical tool for signal analysis. It has become a very important tool for research in the field of mathematics, physics and engineering. It transforms a time domain signal to time-scale domain. This process of transformation is called signal decomposition because a signal is decomposed into several other signals with different level of resolution. Complicated function in terms of small number of coefficients. Often there are less coefficients necessary than in the classical Fourier analysis. Wavelets are adapted to local properties of functions to a larger extent than the Fourier basis. The adaptation is done automatically in view of the existence of a second degree of freedom: the localization in time (or space, if multivariate functions are considered) [15.

The discrete wavelet transforms (DWT) given by Eq. 6 is one of the three forms of wavelet transform.

$$DWTx(m,n) = a_0^{-m/2}\left(\sum_n X(n)\psi \cdot \left[\frac{k - na_0^m b_0}{a_0^m}\right]\right) \quad (6)$$

$X(n)$ is the input, ψ is the *mother* wavelet, asterix in Eq.6 denotes a complex conjugate, a_0^m and $na_0^m b_0$ are the scaling and shifting parameters respectively, $k, m, n \in Z$ (Z is the set of positive integers) [16].

Basically, Multiresolution Analysis (MRA) decomposes a signal into transient details and approximations depending on the similarity with the mother wavelet at each level of resolution (frequency translation). The transients represents high frequency component in the signal, as a result $\{H_0(k-2n)\}_{k=0,1,2,....L-1}$ represents a half band high pass filtering function and $\{G_0(k-2n)\}_{k=0,1,2,....L-1}$ represents a half band low pass filtering function. This type of filter structure is called as the *Quadrature Mirror Filter (QMF)* banks [17]. Basically, the DWT evaluation has two stages. The first consists on the wavelet coefficients determination. These coefficients represent the given signal in the wavelet domain. From these coefficients, the second stage is achieved with the calculation of both the approximated and the detailed version of the original signal, in different levels of resolutions, in the time domain. At the end of the first level of signal decomposition (as illustrated in Fig. 3(a)), the resulting vectors $d_1(n)$ and $a_1(n)$ will be, respectively, the level 1 wavelet coefficients of approximation and of detail. In fact, for the first level, these wavelet coefficients are called $a_1(n)$ and $d_1(n)$, respectively, as stated bellow [16].

$$a_1(n) = \sum_n X(n)G_0(k-2n) \quad (7)$$

$$d_1(n) = \sum_n X(n)H_0(k-2n) \quad (8)$$

Next, in the same way, the calculation of the approximated and the detailed $d_2(n)$ version associated to the level 2 is based on the level 1 wavelet coefficient of approximation $a_1(n)$. The process goes on, always adopting the "n−1" wavelet coefficient of approximation to calculate the "n" approximated and detailed wavelet coefficients. Once all the wavelet coefficients are known, the discrete wavelet transform in the time domain can be determined. This is achieved by "rebuilding" the corresponding wavelet coefficients, along the different resolution levels. This procedure will provide the approximated $a_j(n)$ and the detailed $d_j(n)$ version of the original signal as well as the corresponding wavelet spectrum Fig. 3(b) [16, 18].

4 System description

The proposed cottage PV energy system has the following parts

1. PV array string of series/parallel modules.
2. DC/AC Inverter
3. AC/DC Rectifier for DC motor loads
4. Measurement and recording system (Multiplexer and computer)
5. AC loads : Transformer and 1 phase induction motor
6. DC loads : Separately, shunt, series and compound excited direct current motors

The experiment was set up as a 24 V DC system. Four 12V, 125W PV modules were made up as an array by connecting two sets of two series-connected panels in parallel. A DC–AC inverter of 500 W was used to link the PV cells to the loads. For DC motors, an AC-DC rectifier was used. The electrical wiring connections in the system used 2.5mm^2 copper cables.

5 Experimental Application

Two separate experimental sets have been designed to examine the transient operation of the PV cells feeding electrical machines. The system established for alternating current machines is shown in Fig. 4. As the alternating current machine one-phase induction motor and transformer were separately connected to the system and measurements were made. Experimental system shown in Fig. 5 has been established to examine the effects of transient regime of direct current machines. Measurements have been made for four basic DC machines: serial, shunt, compound and separately excited DC motors. Measurements of both experimental systems have been made with a multiplexer device connected to a computer trough RS-232 communication system. Multiplexer device can take measurements with 0.1 sec intervals and transfer the measurement values to the computer. The values of the current and voltage drawn by each electrical motor from PV batteries have been measured and recorded with 0.1 sec intervals. Measurements have continued until the startup step is completed and steady-state operation is achieved (nearly 11 sec). At the end of the measurements, the obtained current values have been multiplied with the obtained voltage values to find the power drawn from the cells. By making per-unit value conversion, curves showing the power changes trough time have been drawn.

At the end of experimental applications, curves of the changes observed throughput time in the powers drawn at the startup by alternating and direct current electrical machines from PV batteries and their wavelet decompositions are shown in Fig.6, Fig. 7 and Fig. 8 respectively.

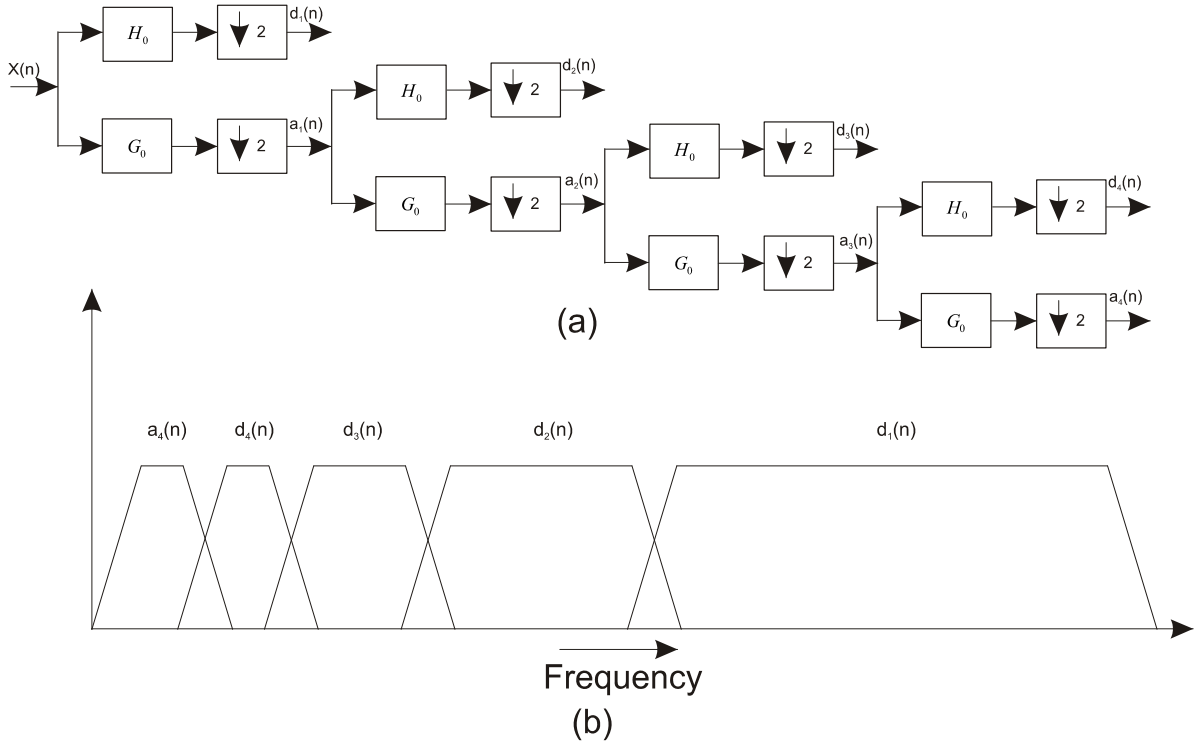

Fig. 3. a) Four level wavelet decomposition tree b) The logarithmic coverage of the DWT

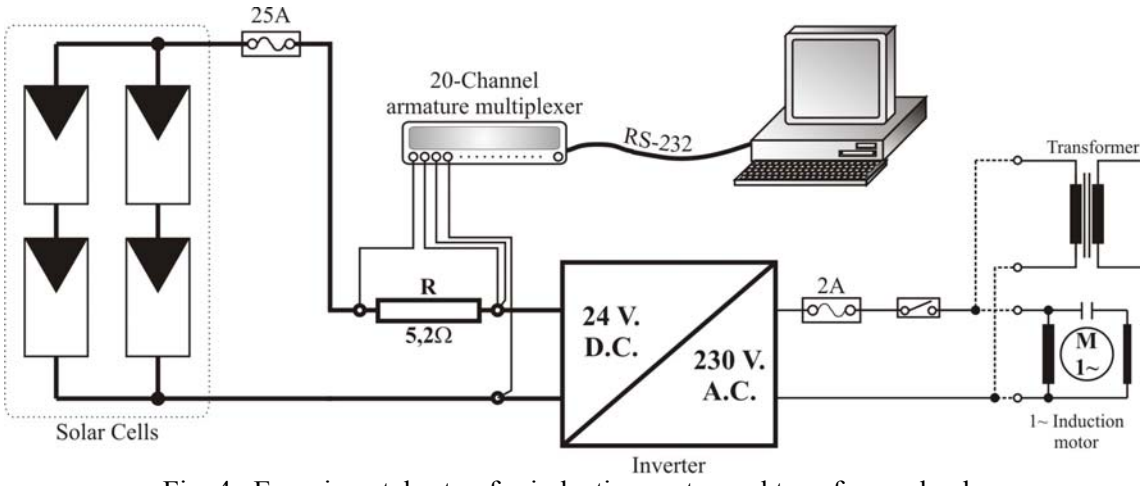

Fig. 4. Experimental setup for induction motor and transformer loads

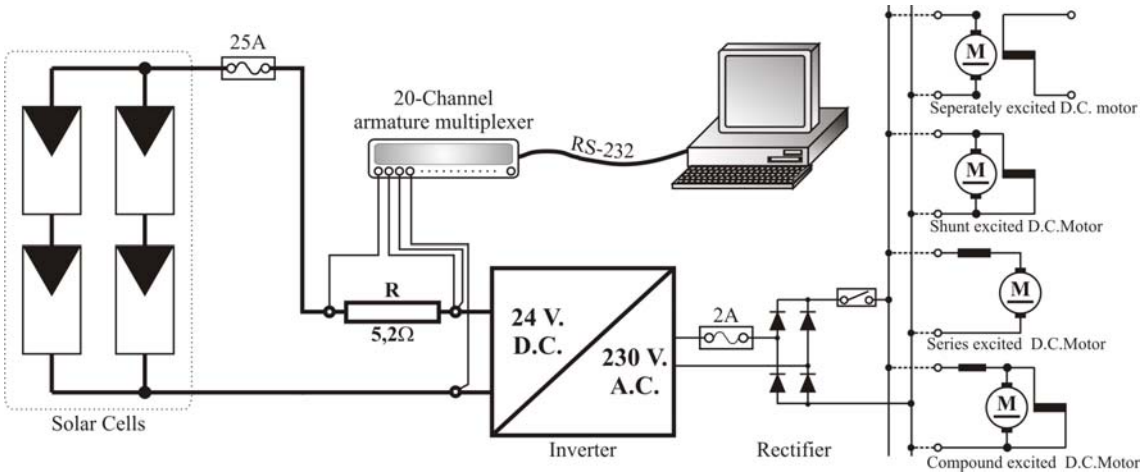

Fig. 5. Experimental setup for DC motor loads

Wavelets can be used as an aid to the detection of features in transient states. Because of nature of MRA, High and low frequency components of the input signals can be obtained. In general, the first level of the wavelet filter bank removes the highest frequency component of the input signal $\left(f_{\max}\right)$, the second removes the frequency $\left(f_{\max}/2\right)$, and third level the frequency $\left(f_{\max}/4\right)$, etc. The sequence of frequency removal is due to the down sampling operation before each filtering operation. This octal shifting in frequency domain is known as frequency translation [17, 18].

Measured input signals' frequency is 10Hz and close to 0. For all electrical machines four level decomposition was carried out and db4 wavelet was preferred for application. At the end of the first level decomposition, detail coefficient $\left(d_1\right)$ frequency range is between 2.5~5Hz, detail coefficient $\left(d_2\right)$ frequency range is between 1.25 ~ 2.5 Hz at second stage, detail coefficient $\left(d_3\right)$ frequency range is between 0.625~1.25Hz at third stage and detail coefficient $\left(d_4\right)$ frequency range is between 0.3125~0.625 Hz and approximation coefficient $\left(a_4\right)$ frequency range is between 0~0.3125 Hz at the last stage.

In Fig. 6 input and decomposition signals of induction motor and transformer are shown. When all decomposition components are examined, transient powers of induction motor except for $\left(d_1\right)$ are bigger than that of transformer. Due to similarity of equivalent circuits and operation principle of these machines, the highest frequency components are very close to each other. On the other hand, lower frequency components acquire different

characters because of air gap and mechanical losses of induction motor.

It can be clearly concluded that induction motor has been the most compelling electrical machine for PV system. This motor has demanded a startup power that is 2.14 times higher than nominal power value. In addition, such demand for quite high power (transient operation period) has lasted for a long time of 8.2 seconds. On the other hand, startup power of transformers has been 1.3 times higher than nominal value. Moreover, the time required to complete transient operation has been only 5.3sec. Continuous ripples in (d_1) and (d_2) originate from load effects of AC machines on PV at continuous state.

When decomposition signals of DC motors (Fig. 7 and Fig. 8) are examined, it is shown that input signals and their decompositions are very similar and there is little difference between each others. Approximations signals values are close to input signals because of low frequency. All decompositions signals of separately excited motor are bigger than that of other DC motors except for the highest harmonic component (d_1). The biggest (d_1) belongs to shunt motor. However other decomposition components $(d_2,\ d_3\ \ d_4\ \ and\ \ a_4)$ of shunt motor are smaller than that of other DC motors. (d_1) components of serial and compound motors are very similar each other but other serial motor decomposition signals are bigger than that of compound motor. Serial motor decomposition signals are second, compound motor decomposition signals are third in magnitude order.

DC motors have also produced similar characteristics in terms of startup power and transient times. While shunt motor has demanded a startup power that is 1.05 times higher than the nominal value, this value has been calculated as 1.1 in serial motor; 1.07 in compound motor; and 1.15 in separately excited motor. When the longest transient time of decomposition signals are examined, transient periods have been calculated as 4sec for shunt motor; 3.8sec for both serial motor; 4sec for compound motor; and 5.4sec for separately excited motor. It has been recorded that particularly transient time separately excited machine has been longer than that of other DC motors. In addition, the demanded startup power has been relatively higher than that of others as well. Such situation results from the fact that nominal excitation current is applied to windings before the motor starts. Thus, the motor starts operating within nominal magnetic field. This, in turn, brings a higher magnetic friction and power loss at the startup. Such situation is not the case in other motors.

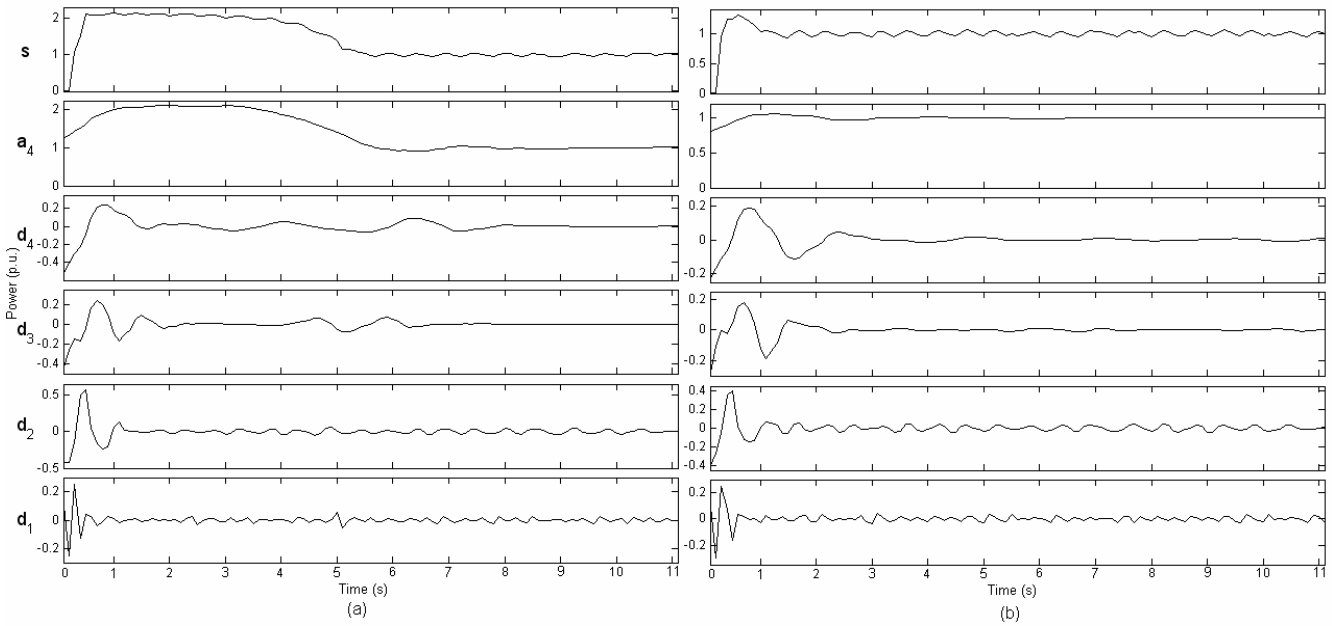

Fig. 6. Decomposition signals a) Induction motor b) Transformer

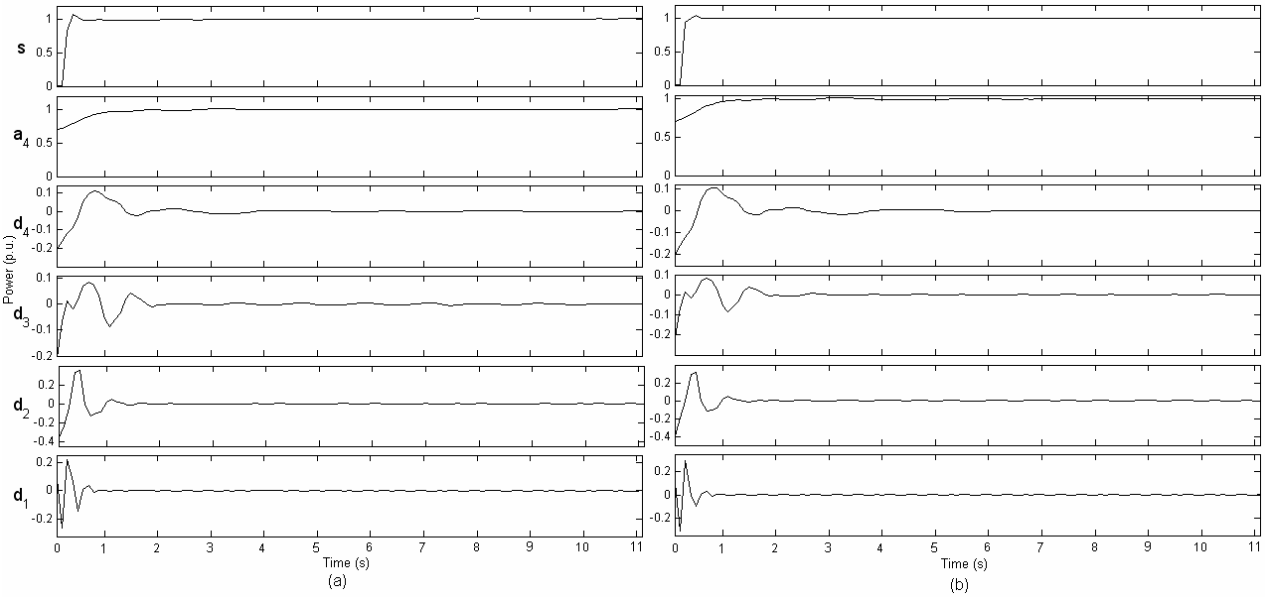

Fig. 7. Decomposition signals a) Serial excited b) Shunt excited

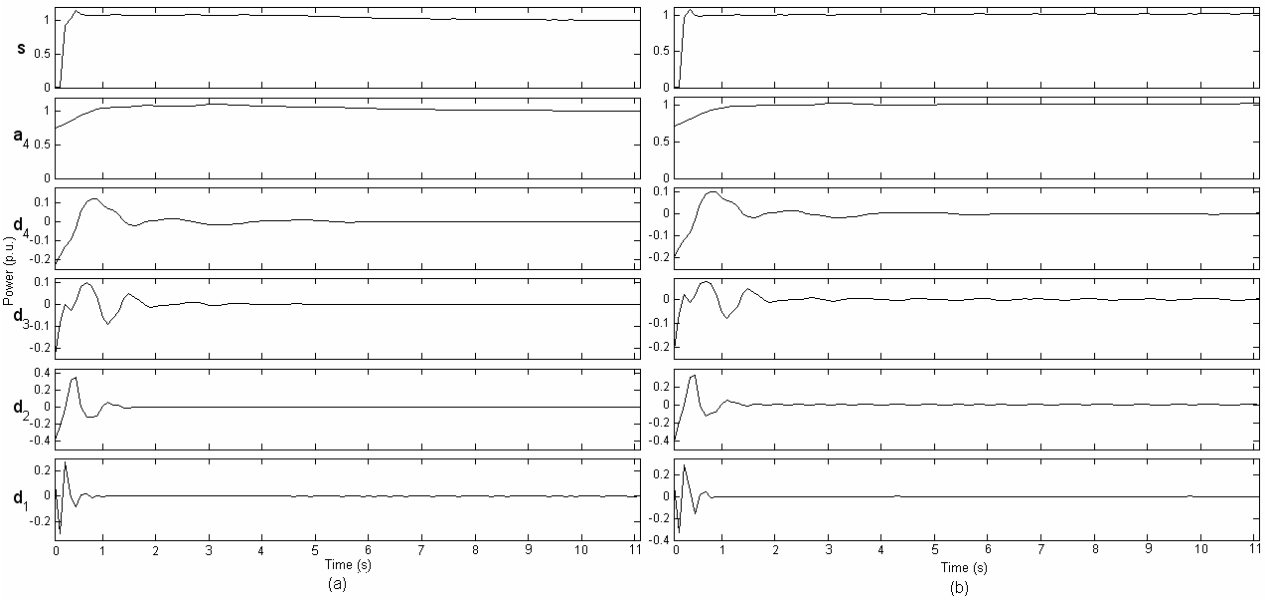

Fig. 8. Decomposition signals a) Separately excited b) Compound excited

7 Conclusion

Photovoltaic systems are designed based on the nominal load of the receiver they will feed. Due to their structural features, the level of the startup current does not have any considerable effect on the photovoltaic in the short run. However, if the startup current is not taken into consideration particularly in the systems that are frequently connected and disconnected, high power drawn may result in over-heating of the modules and decrease of the efficiency of the photovoltaic system. Moreover, power demands that are too high and that last too long may not be met in the systems feeding particularly alternating current machines. In this case, startup performance of the machine will be quite negatively affected. As well as the decrease in the machine efficiency, the efficiency of photovoltaic batteries will decrease more than expected in the long run and their life cycle will be shortened. Therefore, it is of great importance to consider the power quality as well as the power load while designing photovoltaic systems.

Using wavelet transform for transient analysis was useful for comparison of transient power of

electrical machines and detection of certain transient time. While making power detection for the systems composed of alternating current machines, load should be calculated on the basis of a specific value above the nominal operating value and the system should be designed according to such value.

6 Appendix

Table 1. Electrical specifications of PV modules

Rated output (P_{mpp})	125 W
Output tolerance (ΔP_{mpp})	5% / -0%
Guaranteed minimum output ($P_{mpp\ min}$)	125 W
Nominal voltage (U_{mpp})	18,8 V
Nominal current (I_{mpp})	6.65 A
Open circuit voltage (U_{OC})	24.0 V
Short circuit current (I_{SC})	7.27 A
Module efficiency	12.5%
Temperature coefficient α (P_{mpp})	-0.491%/°C
Temperature coefficient β (I_{SC})	+4.7%/°C
Temperature coefficient χ (U_{OC})	-87.4%/°C
Temperature coefficient δ (I_{mpp})	+0.3%/°C
Temperature coefficient ε (U_{mpp})	-91.9%/°C
Normal operating cell temperature (NOCT)	46.6°C
Normal permissible system voltage	600 V
Maximum permissible system voltage	1000 V

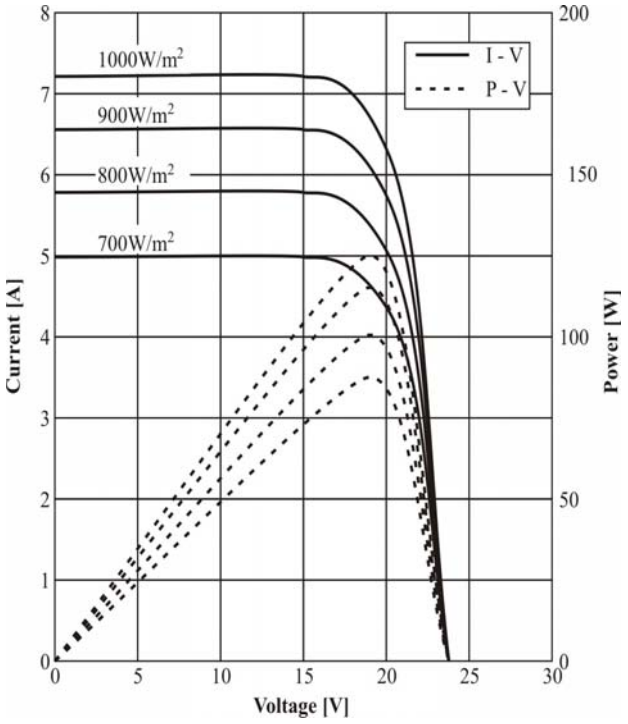

Fig. 9. Electrical performance of solar modules

References:

[1] J. Perlin, *From Space to Earth: The Story of Solar Electricity*, AATCC Publications, Ann Arbor, 1999.

[2] http://www.youthforhab.org.tr, access date: 22.02.2004.

[3] M.R. Patel, *Wind and Solar Power Systems*, CRC Press, U.S.A, 1999.

[4] İ. Güney, N. Onat, Technological Status and Market Trends of Photovoltaic Cell Industry, *WSEAS Transactions on Electronics*, Vol.5, Iss.7, 2008, pp.303-312.

[5] M.A. Green, Photovoltaics: Technology Overview, *Energy Policy*, Vol.28, 2000, pp.989-998.

[6] R. Messenger, J. Ventre, *Photovoltaic System Engineeering*, CRC Press LLC, 2000.

[7] M.A. Green, *Silicon Solar Cells*, Centre for Photovoltaic Devices and Systems, University of South Wales, Sydney, 1995.

[8] C. Rodriguez, G.A.J. Amaratunga, Comparison Between Frequency-Matched and True Sine Wave Grid-Connected Photovoltaic Modules, *in Proc. 6th WSEAS International Conference on Power Systems*, Portugal, 2006, pp.1317-1322.

[9] J. Klima, Closed-Form Analytical Investigation of Space-Vector PWM Inverter Fed Induction Motor Drive under DC-Bus Voltage Pulsation, *WSEAS Transactions on Power Systems*, Vol.3, No.3, 2008, pp.63-75

[10] M. Arrouf, C. Goedel, Photovoltaic Pumping System for Induction Machine with Hysteresis Array Current Control, *IEEE AFRICON 4th*, Vol.2, 1996, pp.853-855.

[11] M. Arrouf, N. Bouguechal, Vector Control of an Induction Motor Fed by a Photovoltaic Generator, *Applied Energy*, Vol.74, 2003, pp.159-167.

[12] S. Singer, J. Appelbaum, Starting Characteristic of Direct Current Motors Powered by Solar Cells, *IEEE Transactions on Energy Conversion*, Vol.8, No.1, 1993 pp.47-52.

[13] H.C. Loyatt, V.S. Ramsden, B.C. Mecrow, Design of an In-Wheel Motor for a Solar-Powered Electric Vehicle, *IEE Proceedings-Electric Power Applications*, Vol.145, Iss.5, 1998, pp.402-408.

[14] S. Enache, A. Bitoleanu, M. Enache, M. Dobriceanu, Stability of Driving Systems with Induction Motors, A New Method for Analysis, *WSEAS Transactions on Circuits & Systems*, Vol.7, Iss.10, 2008, pp.849-858.

[15] N. Vincenzo, Q. Giuseppe, F. Aniello, The Detection of Gear Noise Computed by İntegrating the Fourier and Wavelet Methods, *WSEAS Transactions on Signal Processing*, Vol.4, Iss.3, 2008, pp.60-67.

[16] F. Janicek, M. Mucha, M. Ostrozlik, A New Protection Relay Based on a Fault Transient Analysis Using Wavelet Transform, *Journal of Electrical Engineering*, Vol. 58, No. 5, 2007, pp.271-278,.

[17] S. Saleh, M. Rahman, A New Transient Model for Three-Phase Power Transformers Using a Wavelet Filter Bank, *IEEE Transaction on Power Delivery*, Vol. 20, No.2, 2005, pp.1409-1416.

[18] C.D. Robertson, O.I. Camps, J.S. Mayer, W.B. Gish, Wavelets and Electromagnetic Power System Transients, *IEEE Transaction on Power Delivery*, Vol. 11, No.2, 1996, pp.1050-1058.